IET The Institution of Engineering and Technology WILEY

ORIGINAL RESEARCH

Image restoration with group sparse representation and low-rank group residual learning

Zhaoyuan Cai[1] | **Xianghua Xie[2]** | **Jingjing Deng[3]** | **Zengfa Dou[4]** | **Bo Tong[5]** |
Xiaoke Ma[1]

[1]School of Computer Science and Technology, Xidian University, Xi'an, Shaanxi, China

[2]Department of Computer Science, Swansea University, Swansea, UK

[3]Department of Computer Science, Durham University, Durham, UK

[4]20th Research Institute, China Electronic Science and Technology Group Co., Ltd, Xi'an, Shaanxi, China

[5]Xi'an Thermal Power Research Institute Co., Ltd, Xi'an, China

Correspondence
Xiaoke Ma, School of Computer Science and Technology, Xidian University, Xi'an, Shaanxi, China.
Email: xkma@xidian.edu.cn

Abstract

Image restoration, as a fundamental research topic of image processing, is to reconstruct the original image from degraded signal using the prior knowledge of image. Group sparse representation (GSR) is powerful for image restoration; it however often leads to undesirable sparse solutions in practice. In order to improve the quality of image restoration based on GSR, the sparsity residual model expects the representation learned from degraded images to be as close as possible to the true representation. In this article, a group residual learning based on low-rank self-representation is proposed to automatically estimate the true group sparse representation. It makes full use of the relation among patches and explores the subgroup structures within the same group, which makes the sparse residual model have better interpretation furthermore, results in high-quality restored images. Extensive experimental results on two typical image restoration tasks (image denoising and deblocking) demonstrate that the proposed algorithm outperforms many other popular or state-of-the-art image restoration methods.

1 | INTRODUCTION

Image restoration is one of elementary task in image processing to reconstruct or recovery the original image from the degraded or corrupted signal [1]. It has been extensively studied, in general, can be formulated as

$$Y = HX + E \tag{1}$$

where $X \in \mathbb{R}^{h \times w}$, $Y \in \mathbb{R}^{h \times w}$ and $E \in \mathbb{R}^{h \times w}$ are the original, degraded and noise of image, respectively, and H is a degradation operator. The restoration problem represented in Equation (1) can differ greatly in terms of the degradation operator H. For example, H as an identity matrix corresponds to image denoising [2], a diagonal masking corresponds to image inpainting [3], and a blurring operator corresponds to image deblurring [4].

Evidence demonstrates that image priors are the foundation for image restoration, including total variation (TV) [5–7], sparsity [2, 8], low-rank [9–11], and deep image prior [12–20]. Particularly, sparsity prior is considered as one of the most remarkable for natural images [2, 8, 21–24]. On the basis of the strategies for manipulating sparsity prior, current algorithms are roughly divided into two classes, that is, patch- [2, 25, 26] and group-based approaches [8, 22, 27–29], where the former ones independently perform image restoration for each patch, and the latter ones execute restoration task for each group of patches.

In the past decades, patch-based image restoration has attracted great attention from researchers [2, 30], and those algorithms are devoted to identify the low-dimensional representation (also called patch code) under the assumption that each patch can be modeled with a linear combination of learned basis elements, known as dictionary [2]. The typical dictionary

strategies are classified into two categories, that is, analytic and learning ones, where former one includes discrete cosine transform (DCT), and wavelet and curvelet [31]. In comparison of the traditional analytic approach, dictionary learned from images is more adoptive and accurate since it can depict the local structure of images comprehensively. For example, the well-known dictionary learning method K-SVD [30] is of strong adaptability, which has been successfully applied to image denoising and other tasks [2, 30]. Furthermore, by imposing sparse constraint onto patch representation, patch-based sparse representation (PSR) achieves an excellent performance for image restoration, where each patch is represented with a linear combination of a few atoms of the learned dictionary.

However, those algorithms are criticized for independently learning the dictionary and representation for each patch, resulting in two significant limitations. First, the patch-based methods are computationally time-consuming, hampering its application for large-scale image dataset. Second, these algorithms only exploit the intrinsic structure of each patch but ignores the correlation among various patches [26, 32], namely non-local self-similarity (NSS). To address the named issues, group-based approaches, such as group sparse representation (GSR) [33, 27, 28], learn the sparse coding and dictionary from a group of similar patches, where the strong correlation amongst them can be captured.

Compared to patch-based methods, the GSR models [25, 26] achieve an outstanding performance in image restoration. For example, BM3D [26] performs collaborative filtering on groups of 3D patches. Mairal et al. [33] proposed learned simultaneous sparse coding (LSSC), which given a certain transform domain and simultaneously sparse encodes similar patches to enforce them have similar coefficients. Zhang et al. [27] proposed a GSR-based model for image restoration, which designs the self-adaptive dictionary for image patch group and solves sparse coding with ℓ_0 minimization. Xu et al. [34] learned an NSS prior for patch groups based on external image databases before image denoising, which can achieve excellent results when the distribution of external patch groups and target image patch groups is similar. To preserve the characteristics of the target image itself, a series of models combining internal and external priors are proposed in [35, 36]. To obtain the more correct sparsity solution under image restoration problem, Wang et al. [29] incorporated the nonconvex weighted ℓ_p minimization into GSR framework for image denoising. To avoid learning dictionary from patches of images, principal component analysis (PCA) is adopted to construct dictionary [27, 29]. Recently, Zha et al. [37] proposed low-rank guided GSR model, which utilizes low-rankness to guide dictionary learning. However, due to the degradation of the observed image, the sparse representation obtained by the above methods can't reconstruct the original image faithfully.

To tackle this problem, the residual models [8, 22] assume that the group of similar patches exist the truth representation, where the learned representation should not deviate from the truth one. In contrast to GSR, the residual model is much more difficult to train since it needs to estimate the truth representation, which is also the significant difference among various algorithms. For example, nonlocally centralized sparse representation model (NCSR) [8] utilizes the weighted average of group sparse representation to estimate the true sparse code, whereas NSSRC (for nonconvex structural sparsity residual constraint) [22] integrates structural sparse representation and non-convex sparsity residual constraint for the estimation of truth coding. In addition, the low-rank GSR model (LRGSC) [38] which estimates the true sparse code with low-rank prior is proved to be effective for image compressed sensing in [39].These methods significantly improve the accuracy of algorithms for image restoration, implying that residual model is promising for this issue.

Even though great efforts have been devoted to the residual model for image restoration, there still many unsolved problems. First, the relation among patches of the same groups is neglected since they only depict the distance between the patches and the centers of groups, which decreases the performance and interpretability of patterns. Second, conventional residual models employ the weighted linear function to obtain true sparse representation, where the weights of patches are difficult to select since the relative importance between them and exemplars is hard to measure. Third, the existing algorithms ignore the specificity of patches when estimating the truth representation since they assume that patches within the same group share the same truth representation.

To address these problems, a flexible and interpretable image restoration algorithm based on group sparse representation and residual learning is proposed in this paper. To make use of the relation among patches in the same group and remove the dependence on the exemplars, we define the estimate of the true sparse representation as the product of the learned sparse code and a weight matrix. To adaptively determine the weight matrix, we integrate the learning of weight matrix into self-representation learning, which estimates the weight matrix automatically. Each column of the weight matrix can be different, which enables preservation of the specificity for each patch. In addition, we impose the low-rank constraint on the weight matrix using the nuclear norm, which can further explore the sub-group structures of each patch group. Finally, the proposed algorithm jointly learns the sparse representation, sub-group structure and group residual by combining group sparse representation and residual learning. The experiments imply that the proposed method outperforms many mainstream SOTA methods of image restoration.

The following is a summary of this research's main contributions.

1. To enhance the quality of learned sparse representation, we propose a residual learning model based on self-representation, which makes full use of the relation among patches within the same group. The true sparse representation is estimated by the self-representation of the learned sparse representation, which improves the interpretability of the estimate.

2. To preserve the specificity of the patches within the same group well, we impose the low-rank constraint on the weight

matrix using the nuclear norm, which can further capture the sub-group structures of each patch group.

3. The proposed algorithm jointly learns the patch representation, sub-group structure and group residual by combining group sparse representation and residual learning. In this case, the residual learning assists sparse representation to learn better patch representation, and the sub-group structure of each patch group can ensure that the learned representation preserves the specificity of patches.

4. The experimental results on image denoising and deblocking, imply that the proposed algorithm outperforms many popular image restoration baselines in various quality measurements.

The remaining sections of this article are arranged as follows. Section 2 introduces the preliminaries, Section 3 elaborates the proposed algorithm for image restoration in detail, Section 4 presents the experimental results, and conclusions are drawn in Section 5.

2 | PRELIMINARIES

In this section, we will present the notations and preliminaries that are going to be used for the rest of the paper.

2.1 | Notations

Let the bold upper, bold lower, and lower-case letters denote matrices, vectors, and scalars, respectively. Let $X \in \mathbb{R}^{n \times m}$ be a $n \times m$ matrix, and $x \in \mathbb{R}^{d}$ be a vector with d elements, respectively. X' is the transpose of matrix X.

The Frobenius norm of matrix X is defined as

$$\|X\| = \sqrt{tr\left(X'X\right)} = \sqrt{tr\left(XX'\right)}, \quad (2)$$

where $tr(X)$ is the trace of matrix X. ℓ_0-norm of vector x is defined as the sum of non-zero elements in x, that is

$$\|x\|_0 = \sum_i |x_i|^0. \quad (3)$$

ℓ_1-norm of vector x is the sum of absolute values of elements in x, that is

$$\|x\|_0 = \sum_i |x_i|. \quad (4)$$

ℓ_p-norm $(0 < p < 1)$ of vector x is defined as

$$\|x\|_p = \left(\sum_i |x_i|^p\right)^{1/p}. \quad (5)$$

$\|X\|_0$, $\|X\|_1$ and $\|X\|_p$ denotes imposing ℓ_0-norm, ℓ_1-norm, and ℓ_p-norm on each column of matrix X, respectively.

Nuclear norm of matrix X is defined as

$$\|X\|_* = \sum_{i=1}^{\min(m,n)} |\lambda_i|, \quad (6)$$

where λ_i is the i-th singular value of matrix X.

2.2 | Image restoration

To simplify the model in Equation (1), we set the degradation matrix H as the identity matrix. Then, given a degraded image Y, image restoration is formulated as

$$Y = X + E, \quad (7)$$

where $X \in \mathbb{R}^{b \times w}$ and $E \in \mathbb{R}^{b \times w}$ denote the original image and additive noise, respectively. Without loss of generality, image prior is denoted by θ and then maximum a posteriori (MAP) framework [8, 27, 40] is employed, that is, a posteriori function of the form $\log p(X|Y, \theta)$ is maximized

$$\log p(X|Y) = \log p(Y|X, \theta) + \log p(X|\theta). \quad (8)$$

The likelihood term is the Gaussian distribution [8]

$$p(Y|X, \theta) = \frac{1}{\sqrt{2\pi}\sigma_E} \exp(-\frac{1}{2\sigma_E^2}\|Y - X\|^2), \quad (9)$$

where the σ_E^2 is the variance of noise. And then Equation (8) is equal to

$$\min_{X} \frac{1}{2}\|Y - X\|^2 + \sigma_E^2 \Theta\left(X\right), \quad (10)$$

where $\Theta(X)$ is regularization term derived from prior θ.

2.3 | Sparse representation

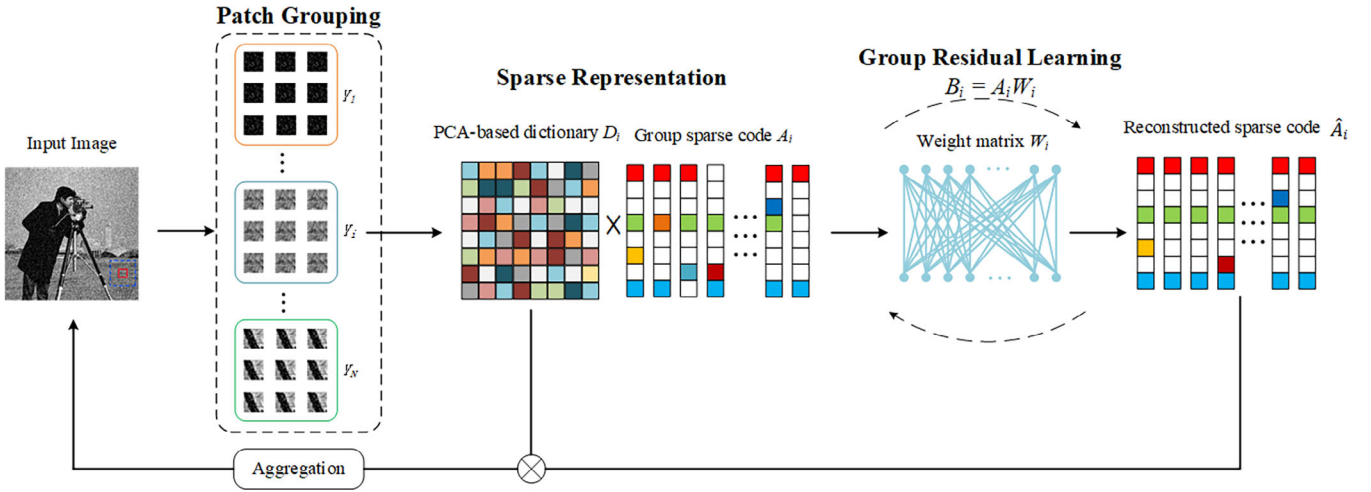Given features $d_1, \dots, d_n$, representation learning for a vector x aims to obtain a linear function such that

$$x \approx a_1 d_1 + \cdots + a_n d_n, \quad (11)$$

where a_i is the coefficient for feature x_i.

Equation (11) is solved by minimizing approximation, that is

$$\min \frac{1}{2}\|x - Da\|^2, \quad (12)$$

where $D = [x_1, \dots, x_n]$, and $a = (a_1, \dots, a_n)'$, respectively.

FIGURE 1 The overview of our proposed image restoration algorithm, which consists of three major parts, namely patch grouping, sparse representation learning and group residual learning.

The sparse representation learning expects most of coefficients are 0, where Equation (12) is formulated as

$$\min \frac{1}{2} \|x - Da\|^2 + \alpha \|a\|_0, \tag{13}$$

where α is a parameter.

Furthermore, extension for sparse representation learning is needed. When multiple objects involve, that is, $X = [x_1, \dots, x_n]$, GSR simultaneously handles n objects into an objective function, where Equation (13) is re-written as

$$\min \frac{1}{2} \|X - DA\|^2 + \alpha \|A\|_0, \tag{14}$$

where $\|A\|_0$ is regularization item, denotes imposing ℓ_0-norm on each column of A.

There are various strategies for constructing sparsity, that is, ℓ_1-norm [41, 42], and ℓ_p-norm ($0 < p < 1$), to bridge ℓ_0 and ℓ_1 [43, 44].

3 | PROPOSED METHOD

In this section, we will present the proposed method in detail, including restoration model, optimization, parameter selection, and discussion on its computational complexity.

The overview of the proposed algorithm is shown in Figure 1, which consists of three major components: patch grouping, sparse representation learning and group residual learning. Patch grouping divides sub-blocks of the original images into different classes, where patches within the same groups are highly similar. Sparse representation learning projects each group of patches into a subspace that spanned by columns of dictionary matrix to obtain the representation of patches, whereas group residual learning aims to automatically learn the true code of patch groups.

3.1 | Restoration model

In the patch grouping block, like other GSR-based restoration models [33, 27, 28], a patch-matching based approach is utilized. Specifically, the degraded image Y is divided into patches, where the size $\sqrt{d} \times \sqrt{d}$ of patches varies with downstream applications. For each reference patch, the closest m patches within window of $l \times l$ are selected as a group, where patches belonging to multiple groups are allowed. To ensure the quality of groups, the step size of selected reference patches is small, where window size is large. In general, we set step size of selection reference patches as 3 or 4, and that of windows as 25×25. By stacking pixels each reference patch is denoted as $\bar{y}_i$, and the corresponding patch group is $Y_i \in \mathbb{R}^{d \times m}$, where each column corresponds to a patch within the group.

In the sparse representation learning block, the most intuitive strategy is to project each group of patches into a subspace, where the low-dimensional representation of patches is obtained. Specifically, given patch group Y_i, the low-dimensional representation of patches is learned by minimizing the approximation, which is formulated as

$$\mathcal{O}(Y_i) = \frac{1}{2} \|Y_i - D_i A_i\|^2, \tag{15}$$

where $D_i \in \mathbb{R}^{d \times d}$ and $A_i \in \mathbb{R}^{d \times m}$ denotes the dictionary and coefficient matrix of Y_i, respectively. Sparse representation learning [30] expects the learned A_i is sparse, that is, the most elements are 0, which improves computational efficiency and interpretability of solutions. By imposing ℓ_1-norm constraint to coefficient matrix A_i, Equation (15) is reformulated as

$$\mathcal{O}(Y_i) = \frac{1}{2} \|Y_i - D_i A_i\|^2 + \beta \|A_i\|_1, \tag{16}$$

where parameter β determines the relative importance of sparsity constraint. Recently, evidence [43, 44] demonstrates that

ℓ_p-norm overcomes limitation of ℓ_1-norm to fulfill sparsity of representation. Therefore, Equation (16) is re-written as

$$\mathcal{O}(Y_i) = \frac{1}{2}\|Y_i - D_i A_i\|^2 + \beta\|A_i\|_p. \qquad (17)$$

However, the coefficient matrix A_i in Equation (17) is very likely to deviate from the true representation of the corresponding group of patches, due to various degradations (noise, compression etc.) on Y_i. Thus, the residual model [8, 22] enforces the learned representation A_i to be in consistent with the truth representation of Y_i. Given the truth representation $B_i \in \mathbb{R}^{d \times m}$ of patch group Y_i, the residual is defined as

$$R_i = A_i - B_i. \qquad (18)$$

Obviously, the learned sparse representation A_i should be as close as possible to the truth sparse representation B_i, that is, R_i should be as small as possible. Thus, Equation (17) can be extended as

$$\mathcal{O}(Y_i) = \frac{1}{2}\|Y_i - D_i A_i\|^2 + \beta\|A_i\|_p + \frac{\gamma}{2}\|A_i - B_i\|^2, \quad (19)$$

where γ determines importance of residual.

The typical advantage of the residual models in Equation (19) is that it learns the low-dimensional representation of patches by preserving the truth distribution of patch group. However, solving Equation (19) is a great challenge. In other words, the dictionary matrix D_i and truth representation B_i are pre-requisites. Usually, principal component analysis (PCA) [27, 8] is a widely adopted strategy to construct dictionary D_i. Specifically, each column of the dictionary D_i consists of the eigenvectors of the Y_i's covariance matrix. However, the truth sparse representation B_i is difficult to estimate, due to we always only have degraded images without ground truth.

To address this problem, existing algorithms assume that patches within each group share the common representation that can be learned from coefficient matrix A_i. The most intuitive and straightforward strategy is to combine the representation of patches with a linear function to obtain the shared truth representation $b \in \mathbb{R}^d$ as [8, 22]

$$b = \frac{1}{m}\sum_{j=1}^{m} w_j A_{i,j}, \qquad (20)$$

where w_i is the weight for patch Y_i as Euclidean distance between the i-th patch and the center of group, and $A_{i,j}$ denotes the j-th column of A_i, respectively. Then, the truth representation set as $B_i = [b, \ldots, b]$.

In comparison to the sparse representation model, the residual model of Equations (19) and (20) is more effective and efficient for image restoration. However, it also has three limitations on the estimation of B_i. First of all, it assumes that patches within the same group share the same truth representation,

ignoring the specificity of patches. In other words, Equation (20) achieves the desirable performance if and only if patches within the same group are homogeneous. Actually, patches groups can be further divided into sub-groups, where each sub-group has a unique representation, indicating that there are multiple representations for the original patch group. Second, the relation among patches of the same groups is also neglected since Equation (20) only depicts the distance between patches and centers of groups decreasing the performance and interpretability of patterns. Furthermore, Equation (20) employs the weighted linear function to obtain B_i, where weights of patches are difficult to select since the relative importance between them and exemplars is hard to measure.

To overcome these issues, we hypothesize that, for each patch group Y_i, there is a close relation between the learned and truth representation of patches, that is, B_i can be learned from A_i. Specifically, the proposed algorithm automatically learns B_i from A_i as

$$B_i = A_i W_i, \qquad (21)$$

where the $W_i \in \mathbb{R}^{m \times m}$ is a weight matrix. Equation (21) avoids sharing the unique center in the residual model in Equation (20), where multiple centers are allowed. In this case, the relations among patches within the same groups are explicitly exploited, which provides a better strategy to characterize and model the truth representation of patches.

Substituting Equation (21) into Equation (19), we have

$$\mathcal{O}(Y_i) = \frac{1}{2}\|Y_i - D_i A_i\|^2 + \beta\|A_i\|_p + \frac{\gamma}{2}\|A_i - A_i W_i\|^2. \qquad (22)$$

Equation (22) brings out three consequent advantages. First, the last term corresponds to the self-representation of learned representation A_i, that is, B_i is represented with linear combination of close patches of groups, improving interpretability of B_i. Second, the relation among patches is further exploited for learning the low-dimensional representation for patches, thereby, enhancing quality of representation in return. Third, the weight matrix W_i is automatically learned under the guidance of the representation of patches, extending the application of models.

Moreover, we also want to explore sub-groups of each patch group with an immediate purpose to further exploit intrinsic structure of representation. Evidence [45] demonstrates the nuclear-norm of matrix ensures the block structure of matrices. Therefore, we fulfil the sub-groups of patch group by imposing constraint on W_i with nuclear norm, then Equation (22) can be reformulated as

$$\begin{aligned} O(Y_i) = &\frac{1}{2}\|Y_i - D_i A_i\|^2 + \beta\|A_i\|_p \\ &+ \frac{\gamma}{2}\|A_i - A_i W_i\|^2 + \tau\|W_i\|_* \\ &s.t. \ W_i = W'_i. \end{aligned} \qquad (23)$$

where τ determines the importance of low-rank constraint. The constraint ensures the symmetry of matrix $\boldsymbol{W}_i$, because each element of $\boldsymbol{W}_i$ can be regarded as similarity between corresponding sparse representations. Equation (24) jointly learns the representation of patches, sub-group structure, and residuals for each patch groups. By summing all patch groups, the proposed algorithm learns representation of patches that is formulated as

$$\mathcal{O}(Y) = \sum_i \mathcal{O}(Y_i). \tag{24}$$

To restore the degraded image, the main model is to minimize the difference between the degraded and restored images, that is, $||\boldsymbol{Y} - \boldsymbol{X}||$. Thus, the overall objective function of the proposed algorithm with the prior regulation terms mentioned above can formulated as

$$
\begin{aligned}
O &= \frac{1}{2}\|Y - X\|^2 + O(X) \\
&= \frac{1}{2}\|Y - X\|^2 + \frac{\alpha}{2}\sum_i \|Q_i X - D_i A_i\|^2 + \beta \sum_i \|A_i\|_p \\
&\quad + \frac{\gamma}{2}\sum_i \|A_i - A_i W_i\|^2 + \tau \sum_i \|W_i\|_* \\
&s.t.\ W_i = W'_i,\ \forall i \in \{1, 2, \ldots, n\},
\end{aligned}
\tag{25}
$$

where $\boldsymbol{Q}_i$ represents the matrix operator for the extraction of the i-th patch group for $\boldsymbol{X}$, that is, $\boldsymbol{Q}_i \boldsymbol{X} = \boldsymbol{X}_i$. In the next subsection, we will discuss the optimization technique for the objective function in Equation (25).

3.2 | Optimization

The nuclear norm of $\boldsymbol{W}_i$ and ℓ_p norm of $\boldsymbol{A}_i$ result in the non-convexity of problem in Equation (25), which cannot be solved directly with analytical solutions. Thus, an alternative iterative strategy is adopted by optimizing one variable by fixing the others until the algorithm converges or termination criteria are reached.

Step 1. *Update weight matrix $\boldsymbol{W}_i$*: By fixing $\boldsymbol{X}$ and $\boldsymbol{A}_i$, and removing irrelevant items, the objective function of Equation (25) is equivalent to the following one with respect to $\boldsymbol{W}_i$, that is

$$\frac{\gamma}{2}\|A_i - A_i W_i\|^2 + \tau\|W_i\|_*\ s.t.\ W_i = W'_i. \tag{26}$$

According to [46], Equation (26) can be effectively solved with singular value decomposition (SVD) of matrix $\boldsymbol{A}_i$, that is, $\boldsymbol{A}_i = \boldsymbol{U}_i \Lambda_i \boldsymbol{V}'_i$, where $\Lambda_i = diag(\{\lambda_i\})$ is a diagonal matrix with singular values on the diagonal, the $\boldsymbol{U}_i$ and $\boldsymbol{V}_i$ are the left and right singular vector matrix, respectively. The optimal solution to Equation (26) is formulated as [46]

$$\hat{W}_i = V_i \mathcal{P}_{\tau/\gamma}(\lambda_i) V'_i, \tag{27}$$

where $\mathcal{P}_{\tau/\gamma}$ is defined as

$$
\mathcal{P}_{\tau/\gamma}(\lambda_i) =
\begin{cases}
1 - \dfrac{\tau}{\gamma\lambda_i^2}, & \lambda_i > \sqrt{\tau/\gamma}, \\
0, & otherwise.
\end{cases}
\tag{28}
$$

Step 2. *Update group sparse representation $\boldsymbol{A}_i$*: By removing other items, the objective function of Equation (25) in terms of $\boldsymbol{A}_i$ is reformulated as

$$\frac{\alpha}{2}\|X_i - D_i A_i\|^2 + \frac{\gamma}{2}\|A_i - A_i W_i\|^2 + \beta\|A_i\|_p. \tag{29}$$

Even though ℓ_p-norm of $\boldsymbol{A}_i$ leads to non-convexity of Equation (29), the generalized soft-thresholding (GST) algorithm [47] provides an efficiently iterative strategy to achieve desired solution. Specifically, the update rule for $\boldsymbol{A}_i$ is formulated as

$$A_i = GST(S_i, \mu, p, t), \tag{30}$$

where t is the number of iterations, $\boldsymbol{S}_i$ and μ are defined as

$$
\begin{cases}
S_i = \alpha\left(A_i - D_i^T X_i\right) + \gamma A_i\left(I - W_i - W'_i + W_i W'_i\right), \\
\mu = \dfrac{\beta}{\alpha + \gamma\|I - W_i\|^2}.
\end{cases}
$$

Step 3. *Update restored image $\boldsymbol{X}$*: By fixing matrix $\boldsymbol{A}_i$ and $\boldsymbol{W}_i$, the restoration of images is formulated as

$$\frac{1}{2}\|Y - X\|^2 + \frac{\alpha}{2}\sum_i \|Q_i X - D_i A_i\|^2. \tag{31}$$

Equation (31) is convex with respect to $\boldsymbol{X}$. By setting the partial derivative of $\boldsymbol{X}$ to zero, the closed-form solution for Equation (31) is deduced as

$$\hat{X} = \left(I + \alpha\sum_i Q'_i Q_i\right)^{-1}\left(Y + \alpha\sum_i Q'_i D_i A_i\right), \tag{32}$$

where $\boldsymbol{D}_i \boldsymbol{A}_i$ denotes the reconstructed patch for $\hat{\boldsymbol{X}}_i$, $\boldsymbol{Q}'_i$ is treated as the operator to put the restored patch back into the original image. Actually, $(I + \alpha\sum_i Q'_i Q_i)$ is a diagonal matrix, whose inverse can be solved at the element-wise division.

Therefore, Equation (32) is interpreted as the weighted average of overlapped reconstructed patches and degraded image to reconstruct the image.

3.3 | Parameter selection

In order to achieve optimal performance results, we also employ the adaptive parameter adjustment strategy to adapt the proposed algorithm to various image structures. First, we update the noise variance σ_E^2 using the iterative regularization strategy [6]

$$\sigma_E^{(k)} = c_0 \sqrt{\left(\sigma_E^2 - \|Y - \hat{X}^{(k)}\|^2\right)}, \qquad (33)$$

where k denotes the k-th iteration and c_0 is a positive constant.

Furthermore, inspired by the maximum a posteriori (MAP) framework [8], we assume that sparse code A_i obeys a hyper-Laplacian distribution [29, 48] and the sparsity residual R_i follows a Gaussian distribution, then we have

$$\beta = \frac{\sigma_E^2}{\delta_i + \epsilon}, \qquad (34)$$

$$\gamma = \frac{\sigma_E^2}{\delta_i^2 + \epsilon}, \qquad (35)$$

where δ_i is the standard variance of A_i, estimated as in [10], and ϵ is a very small constant to avoid dividing by zero.

We also dynamically adjust the parameters α and τ as

$$\alpha = c_1 \, \sigma_E^2, \qquad (36)$$

$$\tau = c_2 \, \delta_i, \qquad (37)$$

where c_1 and c_2 are predefined positive constants. It means that the parameters α and τ are proportional to the noise variance σ_E^2 and standard variance δ_i of A_i, respectively.

3.4 | Method overview

In summary, the proposed algorithm for image restoration can be implemented through the above alternating updating steps and parameter adjustment mechanism. The pseudocode of our proposed algorithm can be found in Algorithm 1.

3.5 | Computational complexity analysis

We further analyze the computational complexity of our proposed method in theory in this subsection. For the space complexity of the proposed algorithm, it requires space $(m^2 n)$. The space for matrix W_i is $O(m^2)$ for each group. The space for matrix A_i and X_i is $O(dm)$ for each group, where d is the number of rows of A_i and X_i. Therefore, the total space complexity of our proposed algorithm is $O(m^2 n)$, where n is the number of groups. For the time complexity analysis of our proposed algorithm, it consists of three major components, that is: 1) group residual learning, 2) sparse representation and 3) reconstruction. The time complexity for updating W_i is $O(tnm^3)$, where

---

ALGORITHM 1 The proposed algorithm for image restoration.

Input: The degraded image Y.

Output: The restored image $\hat{X}$.

1: Initialize $\hat{X}^{(0)} = Y$, $k = 0$, $\sigma_E^{(0)}$.

2: Set the parameters c_0, c_1, c_2 and p.

3: **while** ($k <=$ Max-Iter) **do**

4:     **for** each reference patch x_i in $\hat{X}^{(k)}$ **do**

5:         Search similar patches to construct patch group X_i.

6:         Build dictionary D_i by X_i using PCA.

7:         Update A_i by $A_i = D'_i X_i$.

8:         Update τ by Equation (37).

9:         Update W_i by Equation (27).

10:         Update α, β and γ by Equations (36), (34) and (35).

11:         Update A_i by Equation (30).

12:     **end for**

13:     Update $\hat{X}^{(k)}$ by Equation (32).

14:     Update $\sigma_E^{(k)}$ by Equation (33).

15:     Until the convergence condition is met.

16: **end while**

---

t is the number of iterations. The time complexity for updating A_i is $O(tndm)$. The time complexity for group reconstruction is $O(tnb^2 m)$. Thus, the total time complexity of the proposed algorithm is $O(tnm^3)$.

4 | EXPERIMENTAL RESULTS

To fully validate the performance of the proposed algorithms, extensive experiments are conducted on two typical image restoration tasks: denoising and deblocking. Please find the source code for this research at https://github.com/xkmaxidian/GSR_SRLR_IR.

4.1 | Experimental setting

1. *Benchmark:* As the proposed algorithm is self-supervised learning, only testing data is needed to verify the proposed algorithm performance.

For image denoising task, the benchmark dataset Set12 [49] (including 12 grayscale images) is used to validate the performance with comparisons. The noisy images are synthesized by adding Gaussian noise given a noise level.

For image deblocking, we adopt two widely used datasets: LIVE1 dataset [50] and Classic5 dataset [51], including 29 and 5 natural images, respectively, Compress images are obtained by encoding each test image with the MATLAB jpeg encoder under different compression quality Q and then the JPEG deblocking input images can be generated by a standard JPEG decoder. In addition to LIVE1 and Classic5, we also use 8

TABLE 1 Average PSNR (dB) results of comparison with classic methods for image denoising on the Set12 dataset.

| σ_E	BM3D	EPLL	NCSR	PGPD	aGMM	AST-NLS	GSRC	NSSRC	LGSR	Ours
20	31.01	30.70	31.02	31.02	31.02	31.16	30.93	31.19	31.27	**31.28**
30	29.14	28.75	29.04	29.12	29.08	29.22	29.09	29.28	29.36	**29.40**
40	27.65	27.40	27.65	27.82	27.67	27.81	27.80	27.97	28.04	**28.07**
50	26.72	26.35	26.60	26.81	26.62	26.86	26.81	27.00	27.00	**27.09**
75	24.91	24.48	24.65	24.98	24.67	24.98	25.04	25.15	25.25	**25.28**
100	23.61	23.21	23.29	23.69	23.37	23.71	23.67	23.84	23.95	**23.97**
Average	27.17	26.82	27.04	27.24	27.07	27.29	27.22	27.41	27.48	**27.52**

TABLE 2 Average SSIM results of comparison with classic methods for image denoising on the Set12 dataset.

σ_E	BM3D	EPLL	NCSR	PGPD	aGMM	AST-NLS	GSRC	NSSRC	LGSR	Ours
20	0.8719	0.8681	0.8711	0.8674	0.8716	0.8705	0.8660	0.8736	0.8738	**0.8740**
30	0.8320	0.8223	0.8308	0.8286	0.8290	0.8260	0.8279	0.8339	0.8347	**0.8350**
40	0.7944	0.7827	0.7951	0.7965	0.7909	0.7847	0.7965	0.8030	0.8044	**0.8051**
50	0.7681	0.7475	0.7673	0.7666	0.7569	0.7618	0.7664	0.7780	**0.7798**	0.7784
75	0.7065	0.6738	0.7095	0.7070	0.6832	0.7003	0.7101	0.7219	0.7236	**0.7248**
100	0.6566	0.6154	0.6642	0.6525	0.6230	0.6578	0.6575	0.6807	0.6821	**0.6827**
Average	0.7716	0.7516	0.7730	0.7698	0.7591	0.7669	0.7707	0.7819	0.7831	**0.7833**
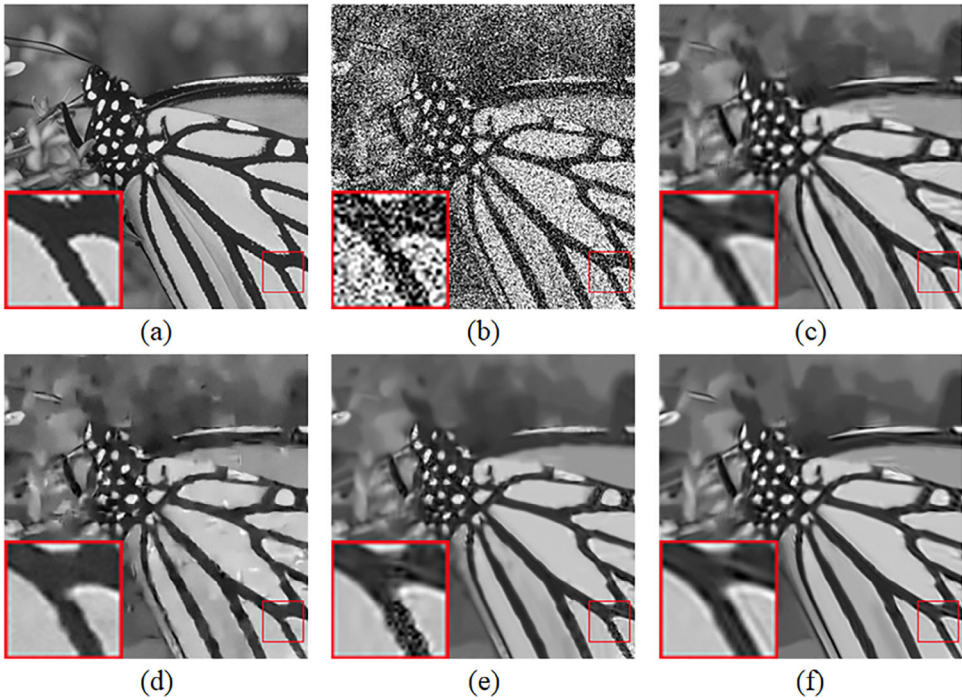
FIGURE 2 The visual comparison denoising results of image Monarch on the Set12 dataset with $\sigma_E = 75$. (a) Original image. (b) Noisy image. (c) BM3D (PSNR = 23.91 dB, SSIM = 0.7557). (d) EPLL (PSNR = 23.72 dB, SSIM = 0.7396). (e) NCSR (PSNR = 23.68 dB, SSIM = 0.7657). (f) Ours (PSNR = 24.38 dB, SSIM = 0.7790).
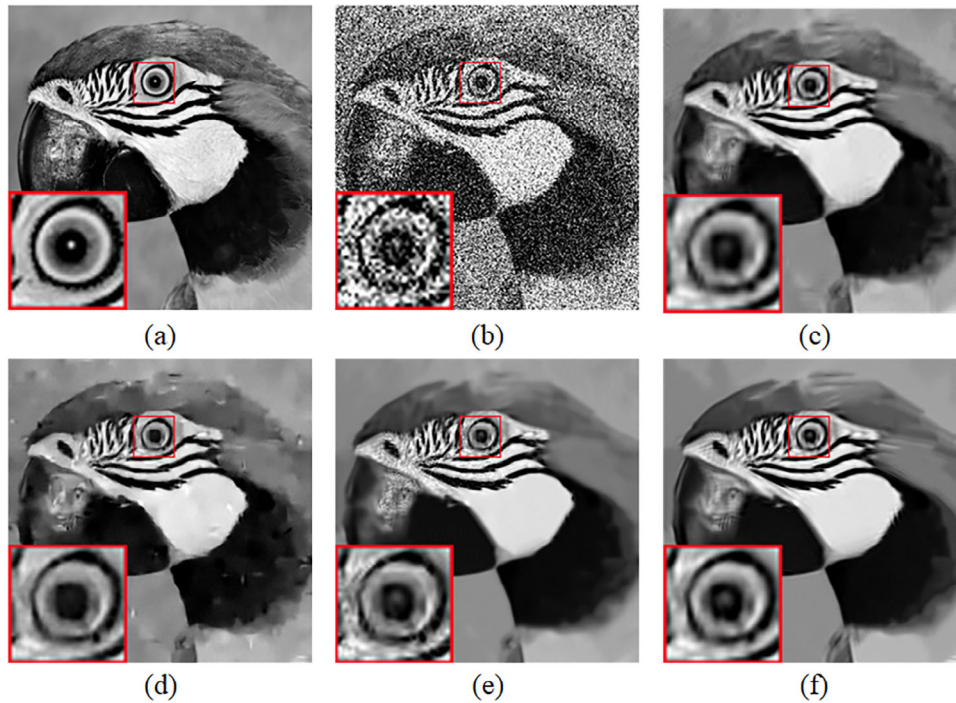
FIGURE 3 The visual comparison denoising results of image *Parrot* on the Set12 dataset with $\sigma_E = 75$. (a) Original image. (b) Noisy image. (c) BM3D (PSNR = 24.19 dB, SSIM = 0.7307). (d) EPLL (PSNR = 24.04 dB, SSIM = 0.7029). (e) NCSR (PSNR = 23.89 dB, SSIM = 0.7363). (f) Ours (PSNR = 24.48 dB, SSIM = 0.7469).

TABLE 3 Average PSNR (dB)/SSIM results of comparison with DNN-based models for image denoising on the Set12 dataset.

Methods	$\sigma_E = 15$	$\sigma_E = 25$	$\sigma_E = 50$	Average
TRND	32.51	30.04	26.78	29.78
	0.8970	0.8523	0.7672	0.8388
DnCNN	32.50	30.17	26.98	29.88
	0.8966	**0.8549**	0.7700	0.8405
S2S	32.07	29.94	26.12	29.38
	0.8891	0.8475	0.7382	0.8249
Ours	**32.65**	**30.24**	**27.09**	**29.99**
	0.8980	0.8535	**0.7784**	**0.8433**

fingerprint images to further verify the superiority of the proposed algorithm.

1. *Parameter setting:* For image denoising, the parameter settings of the proposed algorithm are as follows. The patch size is set to 7×7, 8×8 and 9×9 for $\sigma_E \leq 30$, $30 < \sigma_E \leq 50$ and $50 < \sigma_E \leq 100$. The number of similar patches in a group is set to 60, 70, 80, 90, 100 for $\sigma_E \leq 30$, $30 < \sigma_E \leq 40$, $40 < \sigma_E \leq 50$, $50 < \sigma_E \leq 75$ and $75 < \sigma_E \leq 100$. The parameter p is set to 0.8, 0.85 and 0.9 for $\sigma_E \leq 30$, $30 < \sigma_E \leq 40$ and $40 < \sigma_E \leq 100$.

For image deblocking, the patch size is set to 7×7. The number of similar patches in a group is set to 60. The parameter p is set to 0.9, 0.8 and 0.2 for $Q \leq 10$, $10 < Q \leq 20$ and $20 < Q \leq 40$.

4.2 | Compared methods

In image denoising task, we first compared the proposed algorithm with many SOTA image denoising baselines, including BM3D [26], EPLL [52], NCSR [8], PGPD [34], aGMM [53], AST-NLS [54], GSRC [55], NSSRC [22] and LGSR [37]. These methods are based on sparse representation or image non-local self-similarity prior. Among these methods, NCSR, AST-NLS, GSRC and NSSRC are models based on group sparsity residual, and NSSRC is the SOTA of these methods. In addition, we also compared our proposed algorithm with several deep learning image denoising models, including TRND [56], DnCNN [49], S2S [57], where TRND and DnCNN are supervised learning-based image denoising benchmark algorithms, and S2S is self-supervised learning algorithm.

For image deblocking, we compared our proposed method against BM3D [26], SA-DCT [58], PC-LRM [59], WNNM [60], ANCE [61], SSR-QC [62], COGL [63], JPG-SR [64], NSSRC [22]. To further demonstrate the superiority of our proposed method, we also compared it with several DNN-based image deblocking baselines, including AR-CNN [65], TRND [56], DnCNN [49], DCSC [66], and MDDU (for model-driven deep unfolding method) [67]. Among these competing methods, AR-CNN is the most common deep learning model benchmark for compressed image artifacts removal, the TRND and DnCNN
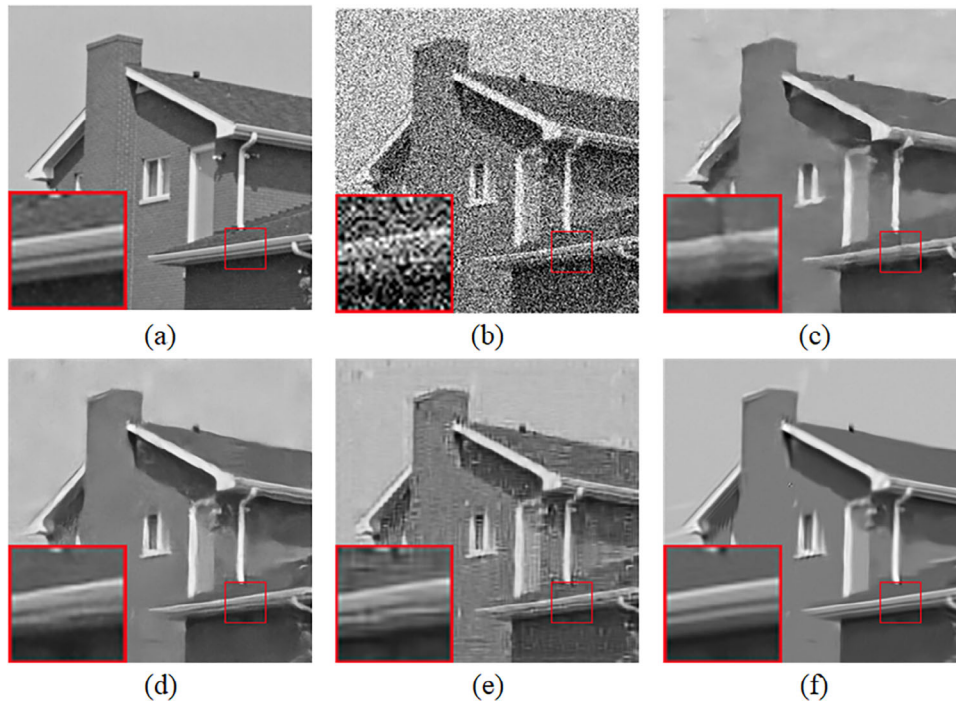
FIGURE 4 The visual comparison denoising results of image *House* on the Set12 dataset with $\sigma_E = 50$. (a) Original image. (b) Noisy image. (c) TRND (PSNR = 29.40 dB, SSIM = 0.8058). (d) DnCNN (PSNR = 29.74 dB, SSIM = 0.8059). (e) S2S (PSNR = 27.47 dB, SSIM = 0.7032). (f) Ours (PSNR = 30.36 dB, SSIM = 0.8221).
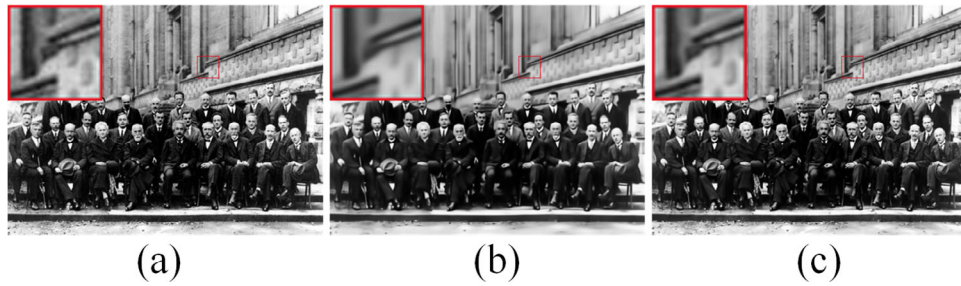

FIGURE 5 The visual comparison denoising results of image *Barbara* on the Set12 dataset with $\sigma_E = 50$. (a) Original image. (b) Noisy image. (c) TRND (PSNR = 25.78 dB, SSIM = 0.7450). (d) DnCNN (PSNR = 25.53 dB, SSIM = 0.7361). (e) S2S (PSNR = 26.82 dB, SSIM = 0.7840). (f) Ours (PSNR = 27.92 dB, SSIM = 0.8231).
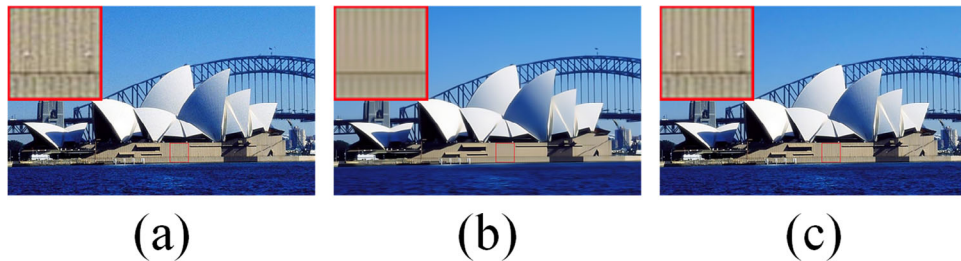
FIGURE 6 The visual results of real image 1 denoising. (a) Real image 1. (b) The result of S2S. (c) The result of our method.

FIGURE 7 The visual results of real image 2 denoising. (a) Real image 2. (b) The result of S2S. (c) The result of our method.

FIGURE 8 The visual results of real image 3 denoising. (a) Real image 2. (b) The result of S2S. (c) The result of our method.

are universal image restoration methods, and the DCSC and MDDU are SOTA image deblocking methods.

It should be emphasized that all comparison methods were tested using the default parameters set by the original authors. In particular, deep learning-based methods were tested using the official pre-training model.

4.3 | Image denoising

Image denoising is the most common and basic image restoration task. In order to verify the effectiveness of our proposed model for image denoising, we use MATLAB's random number generator to synthesize Gaussian White Noise (GWN) images for testing. In addition, we also selected some real images for denoising.

1. *Comparison with classic image denoising methods:* We evaluated all the comparison classic denoising methods using six noise levels: $\sigma_E = 20, 30, 40, 50, 75$, and 100. To quantify the effectiveness of the algorithms, we employ two quality measurements for restored image: PSNR and structural similarity (SSIM) [68]. The image denoising average results on dataset Set12 are summarized in Tables 1 (PSNR) and 2 (SSIM). The best results are highlighted in bold and it is obvious that our proposed algorithm outperforms all other competing methods on both PSNR and SSIM. It is worth noting that our method achieves better performance than other sparsity residual-based methods, especially the NSSRC, where the rationale is two folds. On one hand, the proposed residual learning considers the relation among patches, where the quality of sparse representation in return is enhanced. On the other hand, the weight matrix automatically learned

TABLE 4 Average PSNR (dB) results of comparison with classic methods for image deblocking on the LIVE1 dataset (image size: 256 × 256) and the Classic5 dataset (image size: 256 × 256).

LIVE1 dataset (image size: 256 × 256)

Q	JPEG	BM3D	SA-DCT	PC-LRM	ANCE	WNNM	SSR-QC	COGL	JPG-SR	NSSRC	Ours
10	26.37	27.16	27.23	27.24	27.24	27.25	27.26	27.38	27.29	27.43	**27.45**
20	28.55	29.21	29.24	29.28	29.29	29.29	29.33	29.46	29.37	29.53	**29.54**
30	29.86	30.45	30.48	30.54	30.57	30.55	30.60	30.74	30.75	30.85	**30.87**
40	30.80	31.35	31.37	31.45	31.51	31.46	31.57	31.66	31.71	31.82	**31.84**
Average	28.90	29.54	29.58	29.63	29.65	29.64	29.69	29.81	29.78	29.91	**29.93**

Classic5 dataset (image size: 256 × 256)

| Q	JPEG	BM3D	SA-DCT	PC-LRM	ANCE	WNNM	SSR-QC	COGL	JPG-SR	NSSRC	Ours
10	27.57	28.69	28.72	28.79	28.77	28.78	28.83	28.93	28.78	28.97	**29.03**
20	29.90	30.87	30.89	30.98	30.96	30.98	31.07	31.13	31.12	31.23	**31.26**
30	31.21	32.07	32.09	32.21	32.22	32.21	32.34	32.39	32.50	32.55	**32.58**
40	32.14	32.94	32.96	33.09	33.16	33.10	33.30	33.29	33.46	33.54	**33.54**
Average	30.21	31.14	31.17	31.27	31.28	31.27	31.39	31.43	31.47	31.57	**31.60**

TABLE 5 Average SSIM results of comparison with classic methods for image deblocking on the LIVE1 dataset (image size: 256 × 256)) and the Classic5 dataset (image size: 256 × 256).

LIVE1 dataset (image size: 256 × 256))

Q	JPEG	BM3D	SA-DCT	PC-LRM	ANCE	WNNM	SSR-QC	COGL	JPG-SR	NSSRC	Ours
10	0.7611	0.7877	0.7869	0.7835	0.7879	0.7824	0.7859	0.7957	0.7931	0.7956	**0.7979**
20	0.8423	0.8591	0.8571	0.8550	0.8585	0.8542	0.8576	0.8642	0.8630	0.8645	**0.8658**
30	0.8791	0.8917	0.8903	0.8892	0.8913	0.8888	0.8913	0.8952	0.8967	0.8963	**0.8976**
40	0.8998	0.9103	0.9093	0.9089	0.9102	0.9087	0.9099	0.9129	0.9145	0.9148	**0.9155**
Average	0.8456	0.8622	0.8609	0.8592	0.8620	0.8585	0.8612	0.8670	0.8668	0.8678	**0.8692**

Classic5 dataset (image size: 256 × 256))

Q	JPEG	BM3D	SA-DCT	PC-LRM	ANCE	WNNM	SSR-QC	COGL	JPG-SR	NSSRC	Ours
10	0.7715	0.8087	0.8060	0.8043	0.8081	0.8033	0.8094	0.8134	0.8134	0.8168	**0.8199**
20	0.8519	0.8753	0.8728	0.8723	0.8730	0.8714	0.8740	0.8751	0.8796	0.8802	**0.8811**
30	0.8844	0.9018	0.9002	0.9003	0.9002	0.8998	0.9017	0.9012	0.9063	0.9060	**0.9065**
40	0.9036	0.9178	0.9168	0.9170	0.9172	0.9167	0.9180	0.9175	0.9225	**0.9226**	0.9225
Average	0.8529	0.8759	0.8740	0.8735	0.8746	0.8728	0.8758	0.8768	0.8805	0.8814	**0.8825**
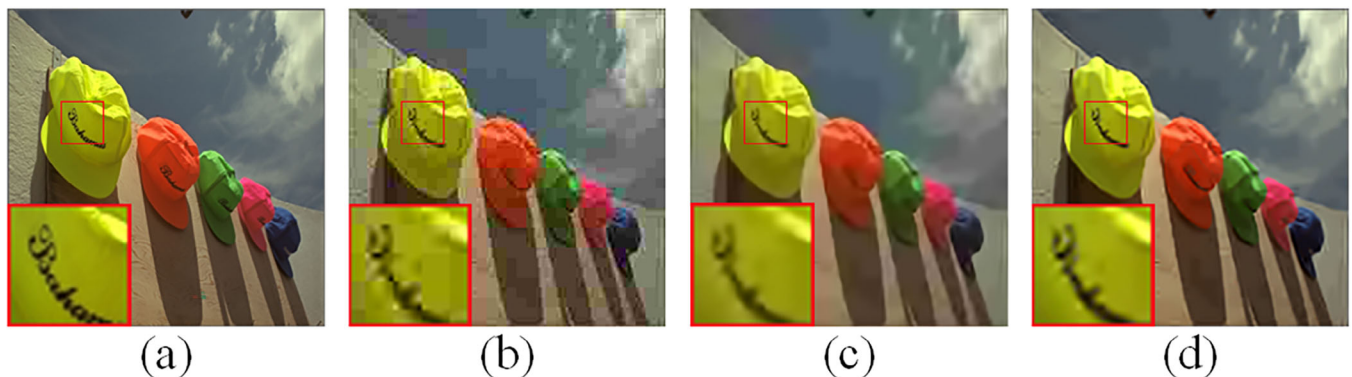
FIGURE 9 The visual comparison deblocking results of image *Caps* on the LIVE1(image size: 256 × 256) dataset at $Q = 10$. (a) Original image. (b) JPEG compressed image (PSNR = 30.75 dB, SSIM = 0.8232). (c) SA-DCT (PSNR = 31.24 dB, SSIM = 0.8634). (d) Ours (PSNR = 31.70 dB, SSIM = 0.8734).
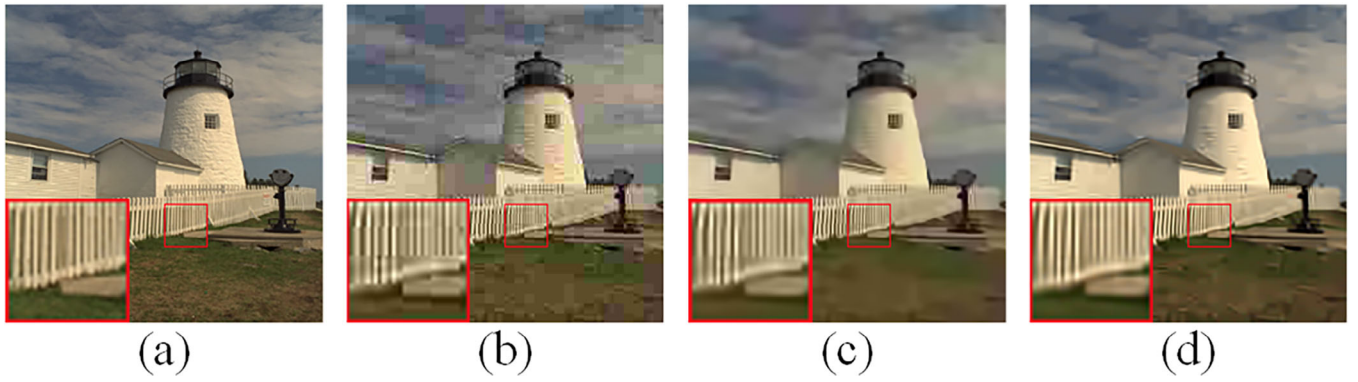
FIGURE 10 The visual comparison deblocking results of image *LightHouse3* on the LIVE1(image size: 256×256) dataset at $Q = 10$. (a) Original image. (b) JPEG compressed image (PSNR = 27.52 dB, SSIM = 0.7561). (c) SA-DCT (PSNR = 28.33 dB, SSIM = 0.7786). (d) Ours (PSNR = 28.78 dB, SSIM = 0.7951).

TABLE 6 Average PSNR (dB)/SSIM results of comparison with DNN-based models for image deblocking on the Classic5 dataset.

Methods	$Q = 10$	$Q = 20$	$Q = 30$	Average
AR-CNN	29.08	31.25	32.60	30.98
	0.7909	0.8514	0.8808	0.8410
TRND	29.29	31.48	32.79	31.19
	0.7996	0.8581	0.8841	0.8473
DnCNN	29.40	31.63	32.91	31.31
	0.8026	0.8610	0.8861	0.8499
DCSC	29.62	31.81	33.06	31.50
	0.8096	0.8641	0.8882	0.8540
MDDU	29.95	32.11	33.33	31.80
	0.8171	0.8689	0.8916	0.8592
Ours	29.36	31.52	32.88	31.25
	0.8041	0.8602	0.8857	0.8500

TABLE 7 Average PSNR (dB)/SSIM results of comparison with DNN-based models for image deblocking on the Fingerprint Images dataset.

Methods	$Q = 10$	$Q = 20$	$Q = 30$	Average
AR-CNN	30.23	33.04	34.76	32.68
	0.8859	0.9291	0.9480	0.9210
TRND	30.42	33.19	34.87	32.83
	0.8899	0.9317	0.9492	0.9236
DnCNN	30.31	33.07	34.73	32.70
	0.8894	0.9308	0.9485	0.9229
DCSC	30.52	33.13	34.78	32.81
	0.8934	0.9330	0.9497	0.9254
MDDU	30.45	32.95	34.35	32.58
	0.8961	**0.9349**	**0.9508**	0.9273
Ours	**30.84**	**33.59**	**35.19**	**33.21**
	0.8971	0.9348	0.9506	**0.9275**

with the low-rank constraint can explore sub-groups of each patch group, which enables the sparse representation learned to preserve the specificity of each patch within the same group.

For further intuitive demonstration, we have made visual comparison with three representative methods: BM3D [26], EPLL [52] and NCSR [8]. BM3D is based on collaborative filtering after block matching, EPLL is based on statistical model (GMM), and NCSR is based on sparse residual model. The visual results on images Monarch and Parrot in Set12 with $\sigma_E = 75$ are presented in Figures 2 and 3, respectively. It can be seen that the images restored by BM3D are blurred or oversmoothed, and the images restored by EPLL and NCSR suffer from undesired visual artifacts. The proposed method not only reduces the noise more effectively than other methods, but also preserves many image details like edges and textures.

1. *Comparison with DNN-based image denoising models:* Deep neural networks (DNN) have achieved great success in various downstream tasks for both high level image understanding and low-level image processing. We therefore compared the proposed algorithm with several mainstream DNN-based image denoising models, including

TRND [56], DnCNN [49], S2S [57]. The PSNR and SSIM results on the Set12 dataset are summarized in Table 3.

Overall, the results show that our proposed method achieves better results even competing with DNN-based methods in image denoising tasks. Selected qualitative results with $\sigma_E = 50$ are illustrated in Figures 4 and 5, in comparison with TRND, DnCNN and S2S. It can be seen that the deep learning-based methods are prone to produce some artifacts or to be oversmoothing, while our method can restore image with more clearly details. Therefore, we conclude that although supervised deep learning can fit diverse image structures with the large training dataset, they hardly to capture the prior of the image itself, such as sparsity and NSS, while our algorithm can make good use of these priors.

FIGURE 11 The visual comparison deblocking results of image *Barbara* on the Classic5 dataset at $Q = 10$. (a) Original image. (b) JPEG compressed image (PSNR = 25.78 dB, SSIM = 0.7621). (c) ARCNN (PSNR = 26.89 dB, SSIM = 0.7934). (d) TRND (PSNR = 27.24 dB, SSIM = 0.8104). (e) DnCNN (PSNR = 27.59 dB, SSIM = 0.8161). (f) Ours (PSNR = 27.91 dB, SSIM = 0.8287).
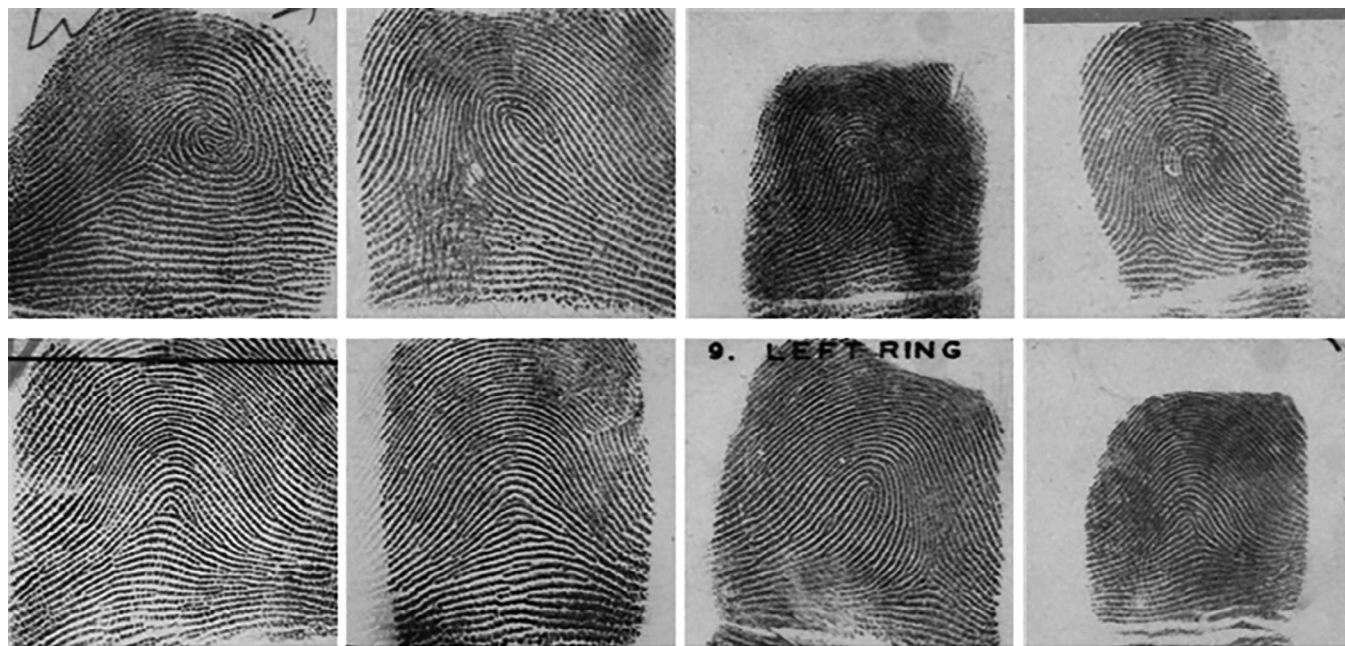

FIGURE 12 The eight fingerprint test images from NIST dataset.

To fully verify the effectiveness of our proposed algorithm, we also selected two real noisy images for experiments. Since our model requires the noise variance of noisy image as a priori, we adopt a fast noise estimation method [69] to obtain the noise variance of the real image in advance. The denoising results are shown in Figures 6–8. We compare our method with the deep learning-based S2S [57] which is also a self-supervised model. It can be clearly seen that the restoration result of S2S is over-smoothed, while our method preserved more image details.
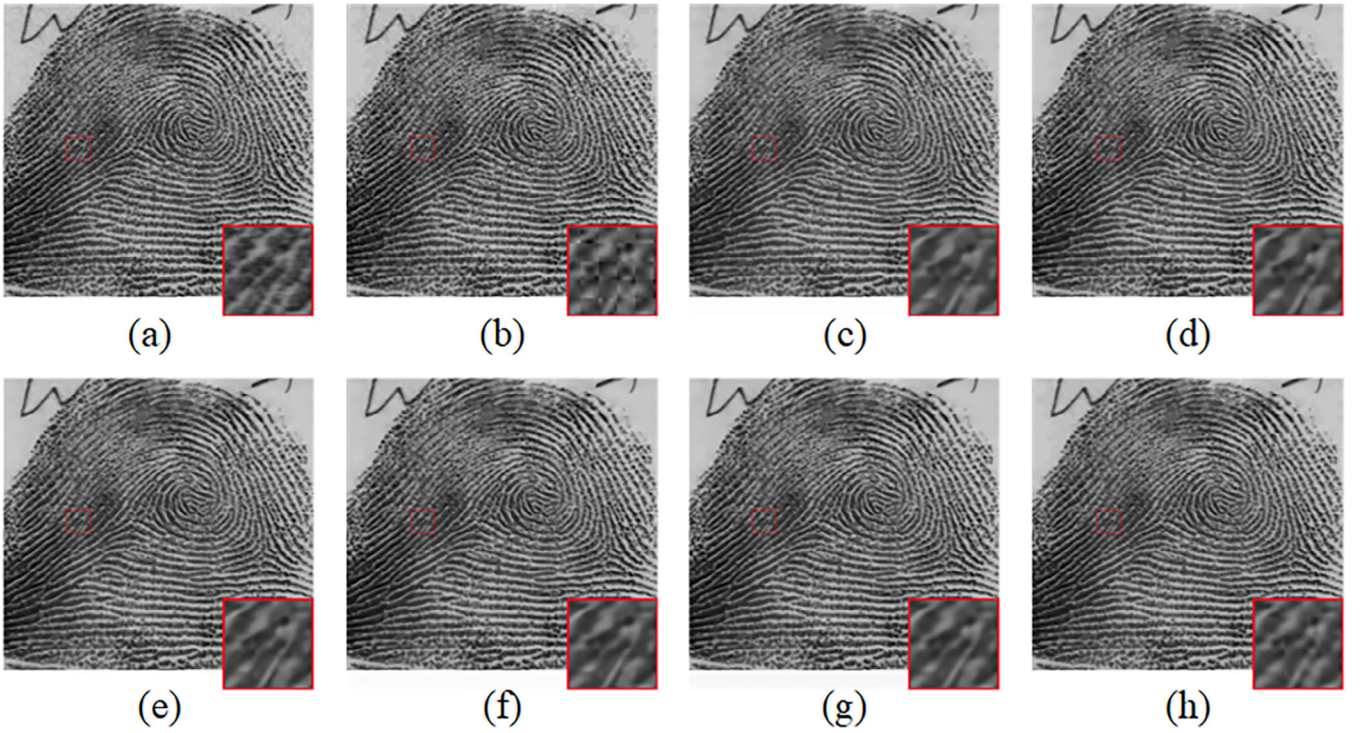
FIGURE 13 The visual comparison deblocking results of *image 01* on the fingerprint dataset at $Q = 10$. (a) Original image. (b) JPEG compressed image (PSNR = 28.41 dB, SSIM = 0.8737). (c) ARCNN (PSNR = 29.57 dB, SSIM = 0.8969). (d) TRND (PSNR = 29.73 dB, SSIM = 0.9008). (e) DnCNN (PSNR = 29.72 dB, SSIM = 0.9019). (f) DCSC (PSNR = 29.82 dB, SSIM = 0.9045). (g) MDDU (PSNR = 29.82 dB, SSIM = 0.9081). (h) Ours (PSNR = 30.17 dB, SSIM = 0.9089).

4.4 | Image deblocking

To further comprehensively verify the effectiveness of our proposed algorithm, we investigated the JPEG deblocking problem [58, 62, 65], reducing the block artifacts in the JPEG compressed images. Different to image denoising, the additive noise E is quantization noise in image deblocking. Thus, we employ a classical Gaussian model [58] which characterizes the noise quantization by estimating the noise standard variance σ_E.

1. *Comparison with classic image deblocking methods:* We evaluated the performance of all competing classic deblocking methods on two public benchmarks: the LIVE1 dataset [50] and the Classic5 dataset [51]. Similar to image denoising, we adopted two evaluation metrics, PSNR and SSIM, and the results are shown in Tables 4 and 5. It is clear that our method outperforms other classical methods apart from SSIM metric on Classic5 with $Q = 40$. In particular, the proposed method is significantly superior to other competing methods on low compression quality images ($Q = 10, 20, 30$), and close to or even exceeds SOTA methods on high compression quality images ($Q = 40$).

The SA-DCT [58] is the most popular image deblocking method, thus we present the visual comparisons shown in Figures 9 and 10. From the qualitative results, we can conclude

TABLE 8 The average computational time (in seconds) of ours method for image denoising and deblocking.

Denoising on 13 widely used test images (256 × 256)				
σ_E	20	40	75	100
Time	136.50	116.49	171.02	249.60
Deblocking on LIVE1 dataset (256 × 256)				
Q	10	20	30	40
Time	81.16	61.68	90.25	69.61

that the proposed method can effectively remove the block artifacts and preserve more image details.

1. *Comparison with DNN-based image deblocking models:* To further demonstrate the advantage of our proposed method on image deblocking task, we also compared it against several DNN-based methods, including AR-CNN [65], TRND [56], DnCNN [49], DCSC [66], and MDDU [67]. The evaluation was carried out on the Classic5 [51] dataset, a popular benchmark for image deblocking. The results of the average PSNR and SSIM with different compression quality Q are listed in the Table 6. It shows that our proposed method achieves better result than AR-CNN and TRND, meanwhile it is comparable to DnCNN, DCSC, and MDDU.

TABLE 9   Average PSNR (dB) results of ablation study on image denoising with the 13 widely used test images.

Modules	$\sigma_E = 20$	$\sigma_E = 30$	$\sigma_E = 40$	$\sigma_E = 50$	$\sigma_E = 75$	$\sigma_E = 100$	Average
SR	31.17	28.57	27.35	27.24	24.87	23.74	27.16
RL	31.08	29.81	28.32	25.90	22.73	23.33	26.86
SR+RL	**32.23**	**30.24**	**28.81**	**27.73**	**25.72**	**24.40**	**28.79**

It is worth noting that these supervised deep learning methods require the large-scale image datasets to train image deblocking model. We notice that if the distribution of the training image dataset and the test images is identical or similar, then the deep learning model can effectively fit diverse image structures.

However, we found that the deep learning method is prone to over-smoothing, especially for images with rich textures, as shown in Figure 11. To further verify this finding, we collected eight fingerprint images from the NIST dataset as a testing benchmark. The eight fingerprint images are shown in Figure 12 and the results for fingerprint image deblocking are summarized in Table 7. Our proposed method achieves better results than all the other competing deep learning-based image deblocking method. The visual comparison examples are shown in Figure 13, where our proposed method can reconstruct better texture details than others.

4.5 | Convergence

It is difficult to provide a theoretical proof for local convergence of our proposed algorithm, due to its patch grouping operations, non-convex optimization, and parameter updates. Therefore, the empirical evidence is provided to verify the convergence of our proposed algorithm. We selected 5 test images from the Set12 dataset, and recorded the process of restoring these images. Figures 14a and 14b show variation curve of PSNR value during algorithm iteration process for image denoising with noise level $\sigma_E = 50$ and image deblocking with compression quality $Q = 10$, respectively. It can be clearly seen that as the algorithm iterates, all PSNR curves of restored images are initially monotonically increasing and then gradually stabilizing. Therefore, the proposed algorithm possesses a good convergence property.

4.6 | Computational time

It is worth noting that our proposed method is based on a group sparse representation model, and each group can be processed independently. Therefore, we implement the algorithm with parallel code in MATLAB. All experiments were run on a laptop with Intel(R) Xeon(R) W-2223 CPU at 3.60 GHz with 32-GB memory. We recorded the average time (in seconds) consumed by our algorithm for denoising on the 13 images of size 256 × 256 shown in Figure 15 and the average time consumed for deblocking on the LIVE1 dataset [50]. The statistical

(a)

(b)
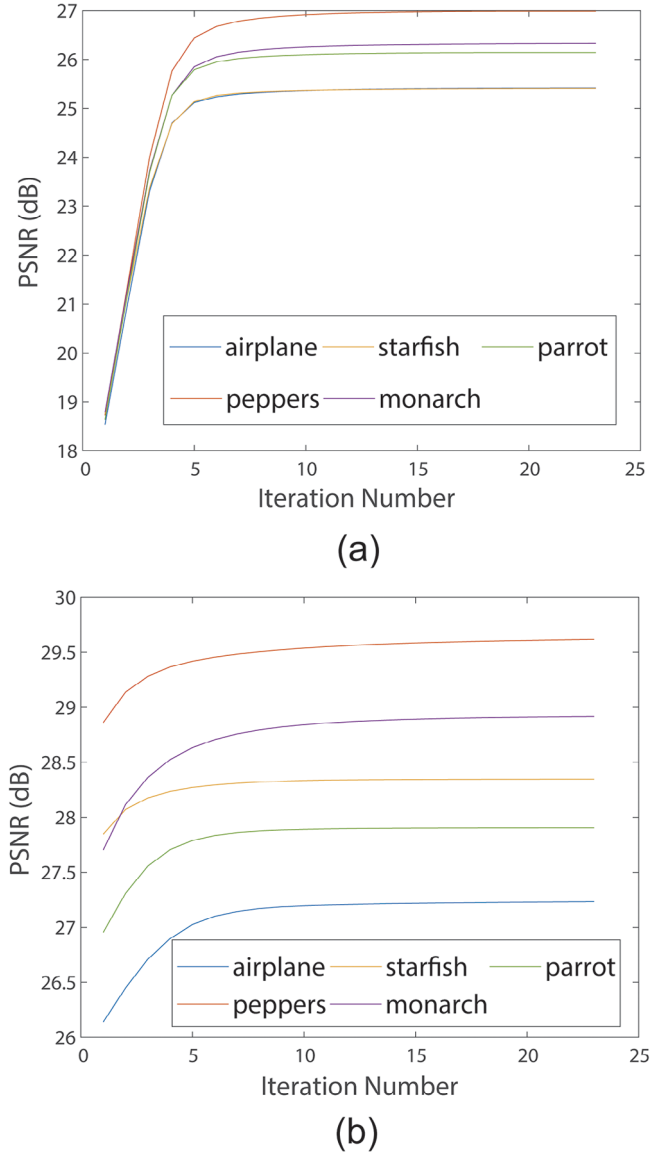
FIGURE 14   Convergence behaviour. (a) PSNR values curve with the number of iterations for image denoising with noise level $\sigma_E = 50$. (b) PSNR values curve with the number of iterations for image deblocking with compression quality $Q = 10$.

results are shown in Table 8. Our algorithm can complete image denoising in 2–4 min, and image deblocking in about 1.5 min. Like other self-supervised algorithms, our method is difficult to achieve real-time, but it is suitable for scenes lacking ground truth (clean images) and high demand for restoration quality.
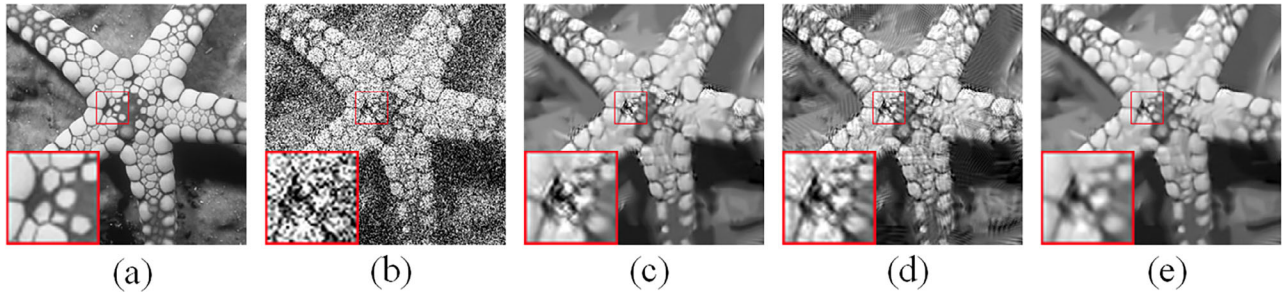
FIGURE 15   The 13 test images used for computational time and ablation study.
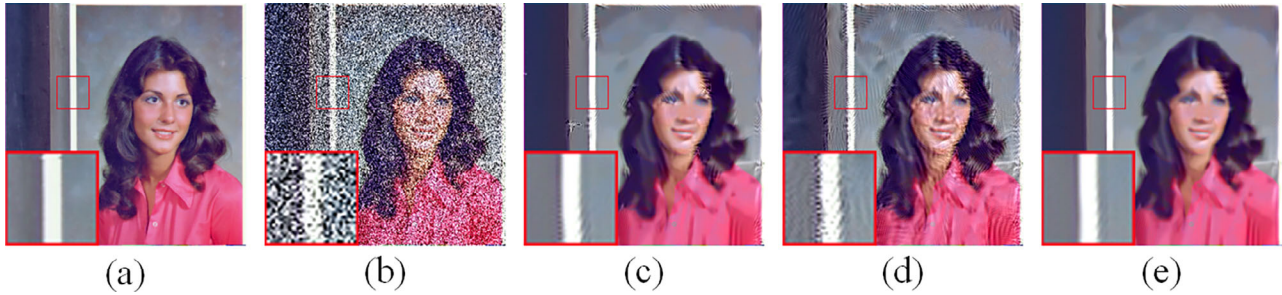
FIGURE 16   The visual comparison denoising results of image *Miss* with $\sigma_E = 75$. (a) Original image. (b) Noisy image. (c) SR (PSNR = 26.38 dB, SSIM = 0.7646). (d) RL (PSNR = 23.52 dB, SSIM = 0.5758). (e) SR+RL (PSNR = 27.61 dB, SSIM = 0.7944).

FIGURE 17   The visual comparison denoising results of image *Starfish* with $\sigma_E = 75$. (a) Original image. (b) Noisy image. (c) SR (PSNR = 23.12 dB, SSIM = 0.6716). (d) RL (PSNR = 21.67 dB, SSIM = 0.5711). (e) SR+RL (PSNR = 23.47 dB, SSIM = 0.6788).

4.7 | Ablation study

To investigate the effectiveness of these different modules in our algorithm, we present the ablation study in this subsection, by removing the group residual constraint ($\gamma = 0$) and the sparsity constraint ($\beta = 0$), respectively. Its variants are simplified into group sparse representation-based restoration model (denoted as SR) and group residual learning-based restoration model (denoted as RL). In order to examine the contributions of SR, RL and our proposed model (SR+RL), we selected 13 test images which are widely used (as shown in Figure 15) and applied these variants to image denoising. The average PSNR results are shown in Table 9. One can observe

that both the group sparse representation and group residual learning play crucial roles in the success of our proposed model.

To further reveal the role of each component of the proposed algorithm, we illustrated some image examples reconstructed by SR model, RL model and the proposed model (SR+RL). As shown in Figures 16c and 17c, the SR model is indeed an ideal image restoration tool, but it can be affected by noise leading to undesirable results. As shown in Figures 16d and 17d, the group residual learning model we proposed can also achieve the purpose of image restoration, but there are many artifacts in the results. Therefore, we consider that SR model provides initial denoising, while RL model provides constraints for

the SR model. The mutual promotion of these two components makes the proposed algorithm successful in image restoration.

5 | CONCLUSION

In this paper, a novel algorithm was proposed for image restoration, where group sparse representation and sparsity residual are simultaneously learned. Unlike conventional sparsity residual models which estimate the true sparse representation using the weighted average method, we first define the estimate of the true sparse representation as the product of the learned sparse representation and a weight matrix, and then our proposed group sparsity residual learning model automatically learns adaptive weight matrix via self-representation learning. Moreover, we explore the sub-group structure of each patch group using the low-rank constraint to better leverage the relation among patches within the same group. The proposed algorithm is comprehensively validated and compared with many other popular or SOTA image restoration methods on public benchmarks. The results demonstrate that, in image restoration tasks such as denoising and deblocking, our suggested approach performs better than those baselines.

However, there are still shortcomings in this work, as it can only handle Gaussian additive noise. In future work, we will consider other distributions of noise, even multiplicative noise.

AUTHOR CONTRIBUTIONS

Zhaoyuan Cai: Data curation; Formal analysis; Investigation; Methodology; Validation; Visualization; Writing—original draft. **Xiaoke Ma** (corresponding author): Conceptualization; Funding acquisition; Supervision; Writing—review & editing. **Xianghua Xie**: Conceptualization; Writing—review & editing. **Jingjing Deng**: Conceptualization; Writing—review & editing. **Zengfa Dou**: Resources; Validation. **Bo Tong**: Resources; Validation.

ACKNOWLEDGEMENTS

CONFLICT OF INTEREST STATEMENT
The authors do not have any possible conflicts of interest.

DATA AVAILABILITY STATEMENT
The data that support the findings of this study are available from the corresponding author upon reasonable request.

ORCID
Zengfa Dou https://orcid.org/0000-0002-5162-6244
Xiaoke Ma https://orcid.org/0000-0002-5604-7137

REFERENCES
1. Banham, M.R., Katsaggelos, A.K.: Digital image restoration. IEEE Signal Process Mag. 14(2), 24–41 (1997)
2. Elad, M., Aharon, M.: Image denoising via sparse and redundant representations over learned dictionaries. IEEE Trans. Image Process. 15(12), 3736–3745 (2006)
3. Yang, J., Wright, J., Huang, T., Ma, Y.: Image super-resolution as sparse representation of raw image patches. In: 2008 IEEE Conference on Computer Vision and Pattern Recognition, pp. 1–8. IEEE, Piscataway (2008)
4. Jung, C., Jiao, L., Qi, H., Sun, T.: Image deblocking via sparse representation. Signal Process.: Image Commun. 27(6), 663–677 (2012)
5. Rudin, L.I., Osher, S., Fatemi, E.: Nonlinear total variation based noise removal algorithms. Phys. D 60(1-4), 259–268 (1992)
6. Osher, S., Burger, M., Goldfarb, D., Xu, J., Yin, W.: An iterative regularization method for total variation-based image restoration. Multiscale Model. Simul. 4(2), 460–489 (2005)
7. Bappy, D., Jeon, I.: Combination of hybrid median filter and total variation minimisation for medical X-ray image restoration. IET Image Proc. 10(4), 261–271 (2016)
8. Dong, W., Zhang, L., Shi, G., Li, X.: Nonlocally centralized sparse representation for image restoration. IEEE Trans. Image Process. 22(4), 1620–1630 (2012)
9. Ji, H., Huang, S., Shen, Z., Xu, Y.: Robust video restoration by joint sparse and low rank matrix approximation. SIAM J. Imag. Sci. 4(4), 1122–1142 (2011)
10. Dong, W., Shi, G., Li, X.: Nonlocal image restoration with bilateral variance estimation: A low-rank approach. IEEE Trans. Image Process. 22(2), 700–711 (2012)
11. Gu, S., Zhang, L., Zuo, W., Feng, X.: Weighted nuclear norm minimization with application to image denoising. In: Proceedings of the IEEE Conference on Computer Vision and Pattern Recognition, pp. 2862–2869. IEEE, Piscataway (2014)
12. Liu, D., Wen, B., Fan, Y., Loy, C.C., Huang, T.S.: Non-local recurrent network for image restoration. In: Advanced Neural Information Processing Systems, vol. 31. MIT Press, Cambridge, MA (2018)
13. Mastan, I.D., Raman, S., Deep, C.F.L.: Deep contextual features learning from a single image. In: Proceedings of the IEEE/CVF Winter Conference on Applications of Computer Vision, pp. 2897–2906. IEEE, Piscataway (2021)
14. Zha, Z., Yuan, X., Zhou, J.T., Zhou, J., Wen, B., Zhu, C.: The power of triply complementary priors for image compressive sensing. In: 2020 IEEE International Conference on Image Processing (ICIP), pp. 983–987. IEEE, Piscataway (2020)
15. Mataev, G., Milanfar, P., Elad, M.: Deepred: Deep image prior powered by red. In: Proceedings of the IEEE/CVF International Conference on Computer Vision Workshops. IEEE, Piscataway (2019)
16. Zamir, S.W., Arora, A., Khan, S., Hayat, M., Khan, F.S., Yang, M.H.: Restormer: Efficient transformer for high-resolution image restoration. In: Proceedings of the IEEE/CVF Conference on Computer Vision and Pattern Recognition, pp. 5728–5739. IEEE, Piscataway (2022)
17. Shen, L., Pauly, J., Xing, L.: NeRP: Implicit neural representation learning with prior embedding for sparsely sampled image reconstruction. IEEE Trans. Neural Netw. Learn. Syst. 1–13 (2022)
18. Chen, L., Chu, X., Zhang, X., Sun, J.: Simple baselines for image restoration. In: European Conference on Computer Vision, pp. 17–33. Springer, Berlin (2022)
19. Zha, Z., Wen, B., Yuan, X., Zhou, J., Zhu, C.: Simultaneous nonlocal low-rank and deep priors for poisson denoising. In: ICASSP 2022-2022 IEEE International Conference on Acoustics, Speech and Signal Processing (ICASSP), pp. 2320–2324. IEEE, Piscataway (2022)
20. Wu, W., Chen, M., Xiang, Y., Zhang, Y., Yang, Y.: Recent progress in image denoising: A training strategy perspective. IET Image Process. 17(6), 1627–1657 (2023)
21. Deeba, F., Kun, S., Ali Dharejo, F., Zhou, Y.: Sparse representation based computed tomography images reconstruction by coupled dictionary learning algorithm. IET Image Proc. 14(11), 2365–2375 (2020)
22. Zha, Z., Yuan, X., Wen, B., Zhang, J., Zhu, C.: Nonconvex structural sparsity residual constraint for image restoration. IEEE Trans. Cybern. 52, 12440–12453 (2021)

23. Yuan, W., Liu, H., Liang, L.: Image restoration via exponential scale mixture-based simultaneous sparse prior. IET Image Proc. 16(12), 3268–3283 (2022)

24. Xu, W., Zhu, Q., Qi, N., Chen, D.: Deep sparse representation based image restoration with denoising prior. IEEE Trans. Circuits Syst. Video Technol. 32(10), 6530–6542 (2022)

25. Buades, A., Coll, B., Morel, J.M.: A non-local algorithm for image denoising. In: 2005 IEEE Computer Society Conference on Computer Vision and Pattern Recognition (CVPR'05), pp. 60–65. IEEE, Piscataway (2005)

26. Dabov, K., Foi, A., Katkovnik, V., Egiazarian, K.: Image denoising by sparse 3-D transform-domain collaborative filtering. IEEE Trans. Image Process. 16(8), 2080–2095 (2007)

27. Zhang, J., Zhao, D., Gao, W.: Group-based sparse representation for image restoration. IEEE Trans. Image Process. 23(8), 3336–3351 (2014)

28. Li, X., Shen, H., Li, H., Zhang, L.: Patch matching-based multitemporal group sparse representation for the missing information reconstruction of remote-sensing images. IEEE J. Sel. Top. Appl. Earth Obs. Remote Sens. 9(8), 3629–3641 (2016)

29. Wang, Q., Zhang, X., Wu, Y., Tang, L., Zha, Z.: Nonconvex weighted ℓ_p minimization based group sparse representation framework for image denoising. IEEE Signal Process Lett. 24(11), 1686–1690 (2017)

30. Aharon, M., Elad, M., Bruckstein, A.K.-S.V.D.: An algorithm for designing overcomplete dictionaries for sparse representation. IEEE Trans. Signal Process. 54(11), 4311–4322 (2006)

31. Daubechies, I.: The wavelet transform, time-frequency localization and signal analysis. IEEE Trans. Inf. Theory. 36(5), 961–1005 (1990)

32. Guo, L., Zha, Z., Ravishankar, S., Wen, B.: Exploiting non-local priors via self-convolution for highly-efficient image restoration. IEEE Trans. Image Process. 31, 1311–1324 (2022)

33. Mairal, J., Bach, F., Ponce, J., Sapiro, G., Zisserman, A.: Non-local sparse models for image restoration. In: 2009 IEEE 12th International Conference on Computer Vision, pp. 2272–2279. IEEE, Piscataway (2009)

34. Xu, J., Zhang, L., Zuo, W., Zhang, D., Feng, X.: Patch group based nonlocal self-similarity prior learning for image denoising. In: Proceedings of the IEEE International Conference on Computer Vision, pp. 244–252. IEEE, Piscataway (2015)

35. Zha, Z., Wen, B., Yuan, X., Zhou, J., Zhu, C., Kot, A.C.: A hybrid structural sparsification error model for image restoration. IEEE Trans. Neural Netw. Learn. Syst. 33(9), 4451–4465 (2021)

36. Yuan, W., Liu, H., Liang, L.: Joint group dictionary-based structural sparse representation for image restoration. Digital Signal Process. 137, 104029 (2023)

37. Zha, Z., Wen, B., Yuan, X., Zhou, J., Zhu, C., Kot, A.C.: Low-rankness guided group sparse representation for image restoration. IEEE Trans. Neural Netw. Learn. Syst. 34(10), 7593–7607 (2022)

38. Zha, Z., Wen, B., Yuan, X., Zhou, J., Zhu, C.: Image restoration via reconciliation of group sparsity and low-rank models. IEEE Trans. Image Process. 30, 5223–5238 (2021)

39. Zha, Z., Wen, B., Yuan, X., Ravishankar, S., Zhou, J., Zhu, C.: Learning nonlocal sparse and low-rank models for image compressive sensing: Nonlocal sparse and low-rank modeling. IEEE Signal Process Mag. 40(1), 32–44 (2023)

40. Niknejad, M., Rabbani, H., Babaie-Zadeh, M.: Image restoration using Gaussian mixture models with spatially constrained patch clustering. IEEE Trans. Image Process. 24(11), 3624–3636 (2015)

41. Candes, E.J., Tao, T.: Near-optimal signal recovery from random projections: Universal encoding strategies? IEEE Trans. Inf. Theory. 52(12), 5406–5425 (2006)

42. Donoho, D.L.: For most large underdetermined systems of linear equations the minimal ℓ_1-norm solution is also the sparsest solution. Commun. Pure Appl. Math. 59(6), 797–829 (2006)

43. Chartrand, R., Yin, W.: Iteratively reweighted algorithms for compressive sensing. In: 2008 IEEE International Conference on Acoustics, Speech and Signal Processing, pp. 3869–3872. IEEE, Piscataway (2008)

44. Mazumder, R., Friedman, J.H., Hastie, T.: Sparsenet: Coordinate descent with nonconvex penalties. J. Am. Stat. Assoc. 106(495), 1125–1138 (2011)

45. Wang, L., Huang, J., Yin, M., Cai, R., Hao, Z.: Block diagonal representation learning for robust subspace clustering. Inf. Sci. 526, 54–67 (2020)

46. Vidal, R., Favaro, P.: Low rank subspace clustering (LRSC). Patt. Recogn. Lett. 43, 47–61 (2014)

47. Zuo, W., Meng, D., Zhang, L., Feng, X., Zhang, D.: A generalized iterated shrinkage algorithm for non-convex sparse coding. In: Proceedings of the IEEE International Conference on Computer Vision, pp. 217–224. IEEE, Piscataway (2013)

48. Krishnan, D., Fergus, R.: Fast image deconvolution using hyper-Laplacian priors. In: Advanced Neural Information Processing Systems, vol. 22. MIT Press, Cambridge, MA (2009)

49. Zhang, K., Zuo, W., Chen, Y., Meng, D., Zhang, L.: Beyond a gaussian denoiser: Residual learning of deep cnn for image denoising. IEEE Trans. Image Process. 26(7), 3142–3155 (2017)

50. Sheikh, H., Wang, Z., Cormack, L., et al.: LIVE imagequality assessment database Release 2. http://live.ece.utexas.educ/research/quality

51. Zeyde, R., Elad, M., Protter, M.: On single image scale-up using sparse-representations. In: International Conference on Curves and Surfaces, pp. 711–730. Springer, Cham (2010)

52. Zoran, D., Weiss, Y.: From learning models of natural image patches to whole image restoration. In: 2011 International Conference on Computer Vision, pp. 479–486. IEEE, Piscataway (2011)

53. Luo, E., Chan, S.H., Nguyen, T.Q.: Adaptive image denoising by mixture adaptation. IEEE Trans. Image Process. 25(10), 4489–4503 (2016)

54. Xiong, R., Liu, H., Zhang, X., Zhang, J., Ma, S., Wu, F., et al.: Image denoising via bandwise adaptive modeling and regularization exploiting nonlocal similarity. IEEE Trans. Image Process. 25(12), 5793–5805 (2016)

55. Zha, Z., Zhang, X., Wang, Q., Bai, Y., Chen, Y., Tang, L., et al.: Group sparsity residual constraint for image denoising with external nonlocal self-similarity prior. Neurocomputing 275, 2294–2306 (2018)

56. Chen, Y., Pock, T.: Trainable nonlinear reaction diffusion: A flexible framework for fast and effective image restoration. IEEE Trans. Pattern Anal. Mach. Intell. 39(6), 1256–1272 (2016)

57. Quan, Y., Chen, M., Pang, T., Ji, H.: Self2self with dropout: Learning self-supervised denoising from single image. In: Proceedings of the IEEE/CVF Conference on Computer Vision and Pattern Recognition, pp. 1890–1898. IEEE, Piscataway (2020)

58. Foi, A., Katkovnik, V., Egiazarian, K.: Pointwise shape-adaptive DCT for high-quality denoising and deblocking of grayscale and color images. IEEE Trans. Image Process. 16(5), 1395–1411 (2007)

59. Ren, J., Liu, J., Li, M., Bai, W., Guo, Z.: Image blocking artifacts reduction via patch clustering and low-rank minimization. In: 2013 Data Compression Conference, pp. 516–516. IEEE, Piscataway (2013)

60. Gu, S., Xie, Q., Meng, D., Zuo, W., Feng, X., Zhang, L.: Weighted nuclear norm minimization and its applications to low level vision. Int. J. Comput. Vision. 121(2), 183–208 (2017)

61. Zhang, X., Xiong, R., Fan, X., Ma, S., Gao, W.: Compression artifact reduction by overlapped-block transform coefficient estimation with block similarity. IEEE Trans. Image Process. 22(12), 4613–4626 (2013)

62. Zhao, C., Zhang, J., Ma, S., Fan, X., Zhang, Y., Gao, W.: Reducing image compression artifacts by structural sparse representation and quantization constraint prior. IEEE Trans. Circuits Syst. Video Technol. 27(10), 2057–2071 (2016)

63. Young, S.I., Naman, A.T., Taubman, D.: COGL: Coefficient graph laplacians for optimized JPEG image decoding. IEEE Trans. Image Process. 28(1), 343–355 (2018)

64. Zha, Z., Yuan, X., Wen, B., Zhang, J., Zhou, J., Zhu, C.: Image restoration using joint patch-group-based sparse representation. IEEE Trans. Image Process. 29, 7735–7750 (2020)

65. Dong, C., Deng, Y., Loy, C.C., Tang, X.: Compression artifacts reduction by a deep convolutional network. In: Proceedings of the IEEE International Conference on Computer Vision, pp. 576–584. IEEE, Piscataway (2015)

66. Fu, X., Zha, Z.J., Wu, F., Ding, X., Paisley, J.: Jpeg artifacts reduction via deep convolutional sparse coding. In: Proceedings of the IEEE/CVF

International Conference on Computer Vision, pp. 2501–2510. IEEE, Piscataway (2019)

67. Fu, X., Wang, M., Cao, X., Ding, X., Zha, Z.J.: A model-driven deep unfolding method for jpeg artifacts removal. IEEE Trans. Neural Netw. Learn. Syst. 33(11), 6802–6816 (2021)

68. Wang, Z., Bovik, A.C., Sheikh, H.R., Simoncelli, E.P.: Image quality assessment: From error visibility to structural similarity. IEEE Trans. Image Process. 13(4), 600–612 (2004)

69. Immerkaer, J.: Fast noise variance estimation. Comput. Vis. Image Underst. 64(2), 300–302 (1996)

How to cite this article: Cai, Z., Xie, X., Deng, J., Dou, Z., Tong, B., Ma, X.: Image restoration with group sparse representation and low-rank group residual learning. IET Image Process. 18, 741–760 (2024). https://doi.org/10.1049/ipr2.12982